UC San Diego
UC San Diego Previously Published Works

Title

Aliphatic and Olefinic Fat Suppression in the Orbit Using Polarity-altered Spectral and Spatial Selective Acquisition (PASTA) with Opposed Phase

Permalink

https://escholarship.org/uc/item/6qw106vq

Authors

Malis, Vadim
Bae, Won C
Yamamoto, Asako
et al.

Publication Date

2023

DOI

10.2463/mrms.mp.2022-0073

Copyright Information

Peer reviewed

MAJOR PAPER

Aliphatic and Olefinic Fat Suppression in the Orbit Using Polarity-altered Spectral and Spatial Selective Acquisition (PASTA) with Opposed Phase

Vadim Malis[1], Won C. Bae[1,2], Asako Yamamoto[3], Yoshimori Kassai[4],
Marin A McDonald[1], and Mitsue Miyazaki[1*]

Purpose: Fatty acid composition of the orbit makes it challenging to achieve complete fat suppression during orbit MR imaging. Implementation of a fat suppression technique capable of suppressing signals from saturated (aliphatic) and unsaturated (olefinic or protons at double-bonded carbon sites) fat would improve the visualization of an optical nerve. Furthermore, the ability to semi-quantify the fractions of aliphatic and olefinic fat may potentially provide valuable information in assessing orbit pathology.

Methods: A phantom study was conducted on various oil samples on a clinical 3 Tesla scanner. The imaging protocol included three 2D fast spin echo (FSE) sequences: in-phase, polarity-altered spectral and spatial selective acquisition (PASTA), and a combination of PASTA with opposed phase in olefinic and aliphatic chemical shift. The results were validated against high-resolution 11.7T NMR and compared with images acquired with spectral attenuated inversion recovery (SPAIR) and chemical shift selective (CHESS) fat suppression techniques. *In-vivo* data were acquired on eight healthy subjects and were compared with the prior histological studies.

Results: PASTA with opposed phase achieved complete suppression of fat signals in the orbits and provided images of well-delineated optical nerves and muscles in all subjects. The olefinic fat fraction in the olive, walnut, and fish oil phantoms at 3T was found to be 5.0%, 11.2%, and 12.8%, respectively, whereas 11.7T NMR provides the following olefinic fat fractions: 6.0% for olive, 11.5% for walnut, and 12.6% for fish oils. For the *in-vivo* study, on average, olefinic fat accounted for 9.9% $\pm$ 3.8% of total fat while the aliphatic fat fraction was 90.1% $\pm$ 3.8%, in the normal orbits.

Conclusion: We have introduced a new fat suppression technique using PASTA with opposed phase and applied it to human orbits. The purposed method achieves an excellent orbital fat suppression and the quantification of aliphatic and olefinic fat signals.

Keywords: *aliphatic and olefinic fat, fat suppression, orbit, polarity altered spectral and spatial acquisition (PASTA), unsaturated and saturated chemical shift opposed phase*

[1]Department of Radiology, University of California San Diego, La Jolla, CA, USA
[2]Department of Radiology, VA San Diego Healthcare System, San Diego, CA, USA
[3]Department of Radiology, Teikyo University, Tokyo, Japan
[4]CT-MR Solution Planning department, Canon Medical Systems Corp., Otawara, Tochigi, Japan

*Corresponding author: Department of Radiology, University of California, San Diego, 9427, Health Sciences Drive, La Jolla, CA 92093-0997, USA. Phone: +1-847-636-7573, Fax: +1-866-387-1895, E-mail: mimiyazaki@health.ucsd.edu
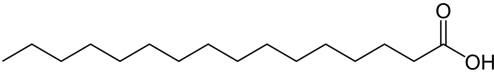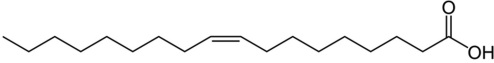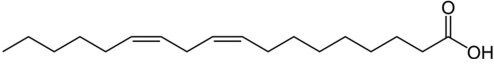
Introduction

The orbit is a highly complex structure with unique and specific physiologic and anatomic properties. Composed of seven bones, the orbit is filled with the eye, lacrimal gland, extraocular muscles, optic nerves, arteries, and veins, all of which are intimately associated with one another through an intricate framework of connective and adipose tissue. Being thus intertwined, disruption of any one of the orbital structures can have potential consequences on the vision and result in significant morbidity.[1] While much attention has been given to orbital pathology trophic for the globes, extraocular muscles, and optic nerves, far less is known

Table 1 Orbital adipose tissue acid composition

Acid		Aliphatic % (# single bonds)	Olefinic % (# double bonds)	Fraction from Ref. #11
Palmitic	$CH_3(CH_2)_{14}COOH$	100% (28)	0% (0)	22–24.6%
Oleic	$CH_3(CH_2)_7\mathbf{CH{=}CH}(CH_2)_7COOH$	94% (28)	6% (2)	45–51.5%
Linoleic	$CH_3(CH_2)_4\mathbf{CH{=}CH}CH_2\mathbf{CH{=}CH}(CH_2)_7COOH$	87% (24)	13% (4)	15–18.6%
Total % (range: min to max)		92.6–94.5	7.4–5.5	

about the potential role of changes in orbital fat quantification, morphology, and content in the normal, aging, and diseased eye.[1] In the daily clinical examination, chemical shift selective (CHESS) fat suppression, short tau inversion recovery (STIR), and Dixon-type opposed phase techniques are used frequently but provide incomplete orbit fat suppression. The drawback of incomplete orbit fat includes unreliability in the detection of tumors embedded in fatty tissue.[2]

In MRI analysis, proton density fat fraction (PDFF) is a noninvasive biomarker for non-alcohol fatty liver disease and accurate estimation of the presence and grading of hepatic steatosis.[3–5] In terms of analyzing fatty acid composition, unsaturated fatty acid components of a methylene-interrupted double bond (-CH=CH-**CH₂**-CH=CH-) and a double bond (-**CH=CH**-) were estimated from the 3D spoiled multi-gradient echo using nine components fat ^{1}H MR spectrum model.[6] The chemical shift-encoded (CSE) MRI was also recently used for quantitative measurements of bone marrow.[7,8] By collecting several CSE imaging data for fat and water separation, it accounts for a full fat spectrum including olefinic fat protons, interrupted protons between two double-bonded carbons, etc.

In general, MR spectroscopy (MRS) at 3T or higher allows for resolving the olefinic protons (at double-bonded carbon sites) resonating at +0.5 ppm from water peak and saturated fatty acid (aliphatic) protons resonating at −3.5 ppm from water. For MRI, there are, of course, many fat suppression techniques that work well to eliminate the signal of aliphatic protons that resonate far from the water peak. Yet, currently, there is no MR imaging technique capable of resolving olefinic protons from the water peak.

In MRI, a basic fat signal such as that from subcutaneous adipose tissue (SAT) and visceral adipose tissue (VAT) resonates at −3.5 ppm from the water peak. Thus, fat suppression techniques like CHESS, spectral inversion recovery (SPIR), spectral adiabatic inversion recovery (SPAIR), and enhanced fat suppression using multiple fat suppression pulses work well in many adipose tissues containing saturated fatty acid.[9,10] The human orbit, however, contains quite a different composition of fatty acids, as compared to SAT and VAT. Orbital adipose tissue (OAT) consists of (Table 1) palmitic acid with saturated fatty acid (22%–24.6%), oleic acid with monounsaturated fatty acid (45%–51.5%), and linoleic acid (15%–18.6%), determined from excised human eyes.[11] The palmitic acid is a saturated fatty acid with a major methylene peak that resonates at −3.5 ppm from the water peak. Of course, palmitic acid has several frequency components other than the methylene peak. Oleic acid has monosaturated protons and linoleic acid has di-unsaturated protons (4 protons at double-bonded carbon sites). Although oleic acid with a single double-bond is abundant in orbits, a long carbon chain of saturated fat or many saturated fat protons is a dominant fatty acid in orbits. Therefore, applying CHESS, SPIR, and SPAIR does not suppress orbit fat completely. In this study, we introduce an orbit fat suppression technique and quantify the relative ratio of olefinic and aliphatic fat in orbits. The technique uses polarity-altered spectral and spatial selective acquisition (PASTA) fast spin echo (FSE) with an olefinic and aliphatic fat opposed phase acquisition to achieve a complete fat suppression to depict optical nerve and surrounding optical muscles.

Materials and Methods

The study protocol consisted of three 2D FSE-based imaging sequences acquired consecutively with the same geometric parameters and receiver gain: i) in-phase images without fat
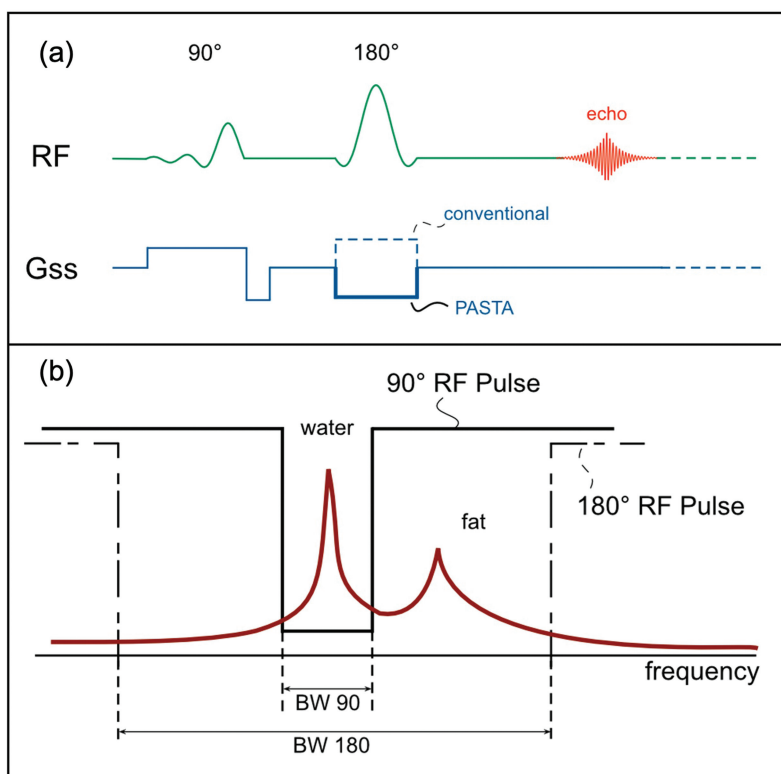
Fig. 1 PASTA pulse sequence diagram using a gradient reversal refocusing pulse (**a**). Spectral selectivity of the 90° pulse and the 180° refocusing pulse in frequency (**b**). BW, bandwidth; Gss, slice selective gradient; PASTA, polarity-altered spectral and spatial selective acquisition.

suppression; ii) with PASTA fat suppression technique depicting water and olefinic fat; and iii) with the combination of PASTA with opposed phase (PASTA & OP) fat suppression techniques, resulting in water-only images.

PASTA

This fat suppression method combines CHESS excitation as part of a spin-echo pulse sequence acquisition with a gradient reversal technique and was first introduced more than two decades ago.[12] A narrow-band spectral-selective 90° RF pulse in conjunction with a reduced strength slice-select gradient is applied, followed by a 180° RF pulse which has a slice-selective gradient applied with the reversed polarity (Fig. 1a). Since fat protons shift out of the slice in different directions between 90° and 180° pulses, only water protons are subject to both the 90° and 180° pulses (Fig. 1b). As a result, fat protons either receive the 90° or 180° pulse, but not both. An overlap ratio of water and fat slices can be written as follows:

$$R = \left(\Delta S - \left| \frac{\Delta f_{fat}}{G_{90}} - \frac{\Delta f_{fat}}{G_{180}} \right| \right) \cdot \frac{1}{\Delta S} \approx 1 - |\Delta f_{fat}(\tau_{90} + \tau_{180})| \quad (1)$$

where ΔS is a slice thickness, Δf_{fat} is chemical shift of fat, and magnitude of the gradients corresponding to 90° and 180° RF pulses is $G_{90,180} = 1/(\tau_{90,180} \cdot \Delta S)$; full derivation is provided in the Appendix.

Olefinic aliphatic opposed phase

Figure 2 shows pulse sequence diagrams of a) in-phase, b) PASTA, and c) PASTA & OP. Although PASTA is a water excitation technique, some aliphatic fat signals evolve during TR and multiple slices. This residual signal of aliphatic fat can be canceled with the opposed phase. The opposed phase method is an asymmetric spin-echo technique in which the data for the echo center are acquired at the time when the signals from water and fat are out of phase.[13] In PASTA & OP, we utilize the chemical shift directly between the aliphatic and olefinic fat which is about 4 ppm at 3T (olefinic proton resonating at 5.3 ppm and aliphatic proton at 1.3 ppm), translating to 504 Hz. Thus, for the opposed phase method, corresponding 0.98 ms shift is introduced into the sequence for imaging gradients after the 180° pulse (Fig. 2c).

Fat quantification

Aliphatic and olefinic fat fraction colormaps were estimated as following: each voxel inside the ROI must satisfy the following condition:

$$S_{IP} > S_{PASTA} > S_{PASTA \& OP}$$

where S_{IP} is in-phase signal intensity, S_{PASTA} is PASTA signal intensity, and $S_{PASTA \& OP}$ is PASTA & OP signal intensity. Fat signal is calculated by subtracting $S_{PASTA \& OP}$ (water-only image) from the S_{IP} in-phase images (water and fat):
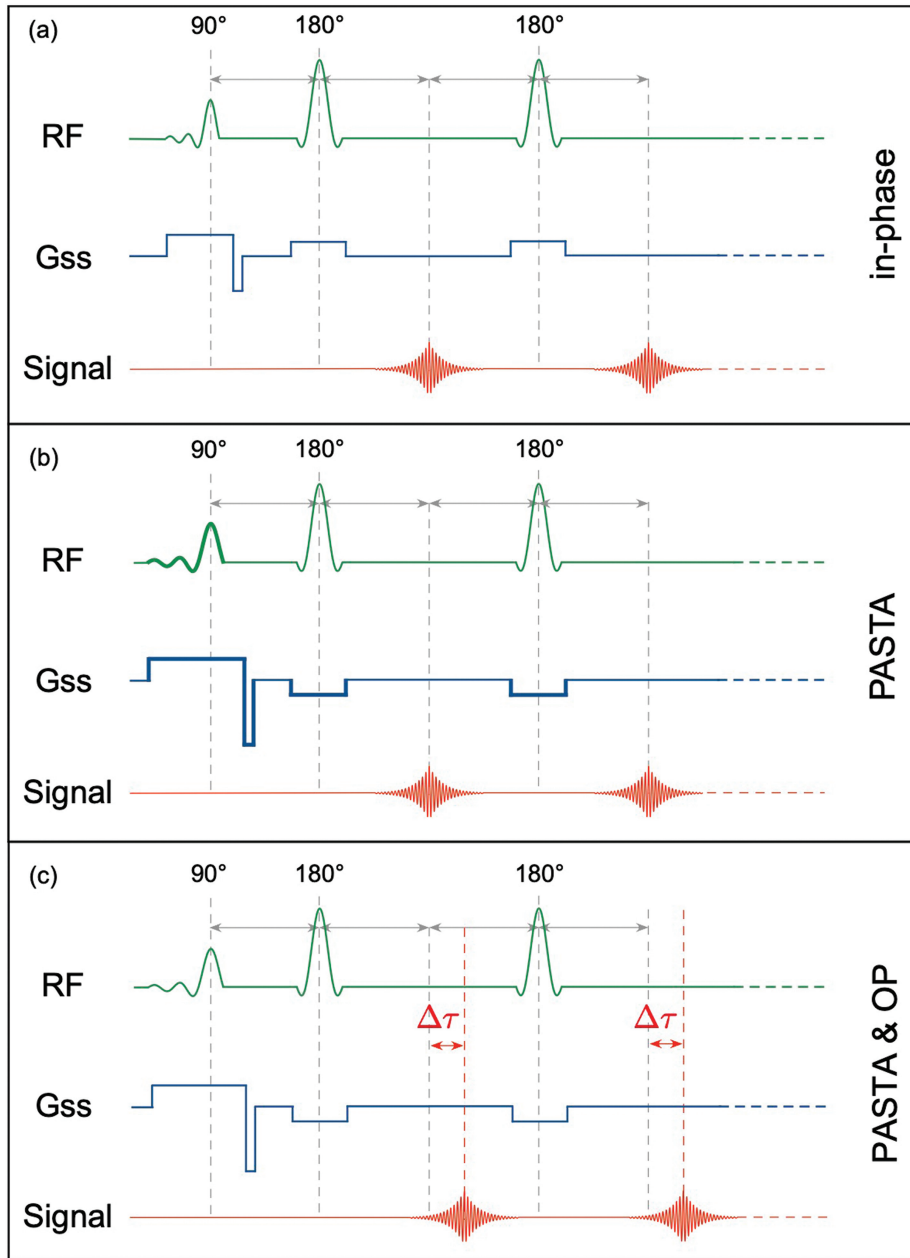
Fig. 2 Simplified diagrams of FSE sequences (**a**) in-phase, (**b**) PASTA (note the wider 90° RF for frequency selective pulse and reversal of slice select gradients [indicated in bolder lines for RF and G_{ss}]), (**c**) PASTA & OP: chemical shift $\Delta\tau$ to be an out-of-phase is introduced. FSE, fast spin echo; Gss, slice selective gradient; OP, opposed phase; PASTA, polarity-altered spectral and spatial selective acquisition.

$$S_{fat} = S_{IP} - S_{PASTA \ \& \ OP} \tag{2}$$

Aliphatic fat signal can be calculated as difference between in-phase image (water and fat) and PASTA image (water and olefinic fat):

$$S_{alp} \approx S_{IP} - S_{PASTA} \tag{3}$$

Finally, the olefinic fat signal is:

$$S_{olf} = S_{fat} - S_{alp} \tag{4}$$

The % ratio of aliphatic and olefinic fat is simply:

$$F_{alp} = \frac{S_{alp}}{S_{fat}} \cdot 100\% \tag{5.1}$$

$$F_{olf} = \frac{S_{olf}}{S_{fat}} \cdot 100\% \tag{5.2}$$

The above calculations are limited by only relying on the residual aliphatic fat signal after the PASTA excitation. In addition, since all fatty acids have the same triglyceride backbone compositions resonating between 4 ppm and 4.5 ppm, we ignored them. As for the T_2 relaxation effect,
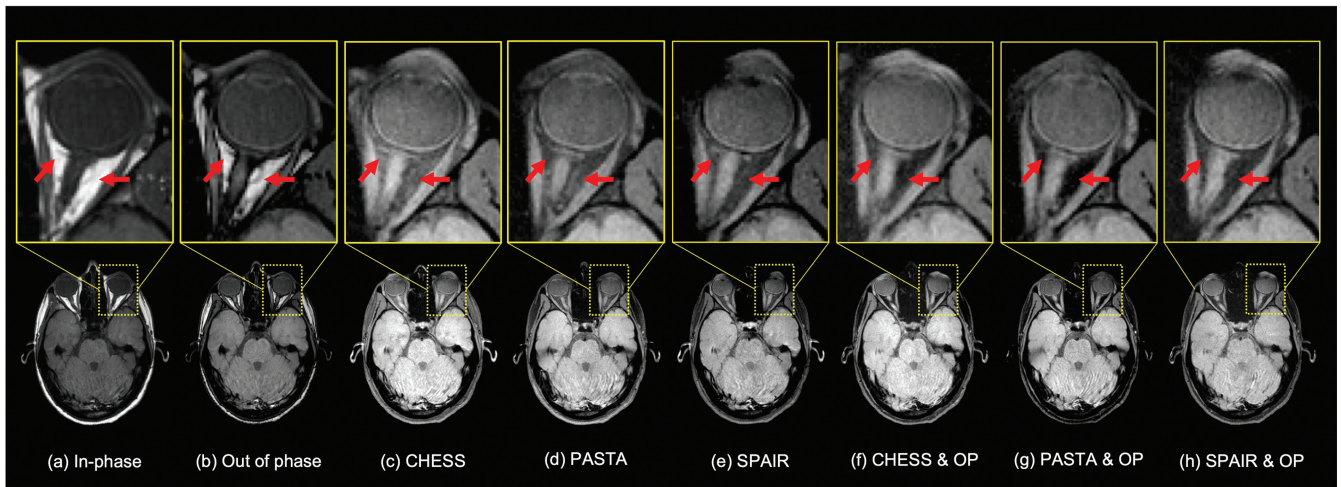
Fig. 3 Axial images with enlarged orbit regions, red arrows highlighting orbital adipose regions: (**a**) In-phase, (**b**) Out of phase, (**c**) CHESS, (**d**) PASTA, (**e**) SPAIR, (**f**) CHESS & OP, (**g**) PASTA & OP, and (**h**) SPAIR & OP. Note that out of phase cancels water and aliphatic fat signals within the pixel. CHESS, SPAIR, and water excitation of PASTA also show remaining olefinic fat signals. Only the PASTA & OP technique shows complete fat-suppressed images of orbits with well-delineating optical nerve and extraocular muscles. CHESS, chemical shift selective; OP, opposed phase; PASTA, polarity-altered spectral and spatial selective acquisition; SPAIR, spectral adiabatic inversion recovery.

it is important to mention that T_2 values of various fatty acid peaks are reported to be 44–55 ms, except methyl protons of 80 ms.[14] In the present study, δTE, the chemical shift difference between in-phase and out-phase, is 0.98 ms. That is much shorter than T_2 values of fatty acids; therefore, an error caused by T_2 of fatty acids is negligible and can be estimated to be about 1%.[15]

Phantom study

A phantom study was conducted prior to the *in-vivo* experiment. Bottles of olive, fish, and walnut oils were purchased from a local grocery store and scanned on a clinical scanner (Vantage Galan 3T; Canon Medical Systems, Tochigi, Japan) using a 32-channel brain coil. The oils were poured into 50 mL test tubes and placed together with the identical test tube filled with water. Collected images were used to estimate olefinic and aliphatic fat fractions of oil phantoms. To confirm the accuracy of the purposed method, high-resolution proton-nuclear magnetic resonance (NMR) experiments were carried out for three samples made from olive, fish, and walnut oils. 10 mg of each of the oils solubilized in 600 μL of deuterated solvent were scanned with 500 Varian VX system (500 MHz, 11.7T; Varian, Palo Alto, USA).

In-vivo measurements

In-vivo imaging was performed after Internal Review Board (IRB) approval with a clinical scanner (Vantage Galan 3T) on eight adult subjects (53 $\pm$ 15 y.o.; 7 males and 1 female) using a 32-channel brain coil. Similar to the phantom study, the protocol included three sequences: all series were acquired with the same receiver gain and shared the following parameters: TE/TR = 15/1000 ms, NEX = 1, FA = 90°,

axial orientation FOV = 22 × 22 cm, matrix size 320 × 320, and 16 slices of 3 mm thickness, the total scan time for all three series was 6 min and 30 sec. The parameters of RF pulses were: (a) in-phase excitation RF pulse was an asymmetric sinc 5:1, duration 5.75 ms; (b) PASTA FA = 95° with an asymmetric sinc 5:1 pulse, duration 7.2 ms; and (c) refocusing 180° RF pulses were same for all the sequences using a symmetric sinc with a single lobe and duration 2 ms; all pulses were centered at water peak of 4.7 ppm. The duration of the excitation and refocusing pulses in PASTA were set according to equation (1). We optimized the flip angles of PASTA (varying from 90° to 120° in steps of 5°). All other parameters were set to default and no further optimization was performed for other fat suppression techniques. An axial slice for quantification was chosen to have the largest orbital cross-section and include an optical nerve. Prior to the analysis, *in-vivo* images were registered with the corresponding in-phase images using 2D rigid body registration with three degrees of freedom. Two ROIs containing orbital fat were identified from the axial slice for fat fraction map calculation. Low signal voxels corresponding to optical nerve were automatically excluded from the ROI. Quantitative results were obtained for two circular ROIs (r = 5 px) placed inside the large orbital ROIs. To test the reproducibility of the measurements, the scanning protocol was repeated on a subgroup of two subjects on a different day.

Results

Figure 3 shows the fat suppression effect of orbit using a) In-phase, b) Out of phase, c) CHESS, d) PASTA only, e) SPAIR only, f) CHESS & OP, g) PASTA & OP, and f) SPAIR & OP. Note that the opposed phase takes care of the cancellation of
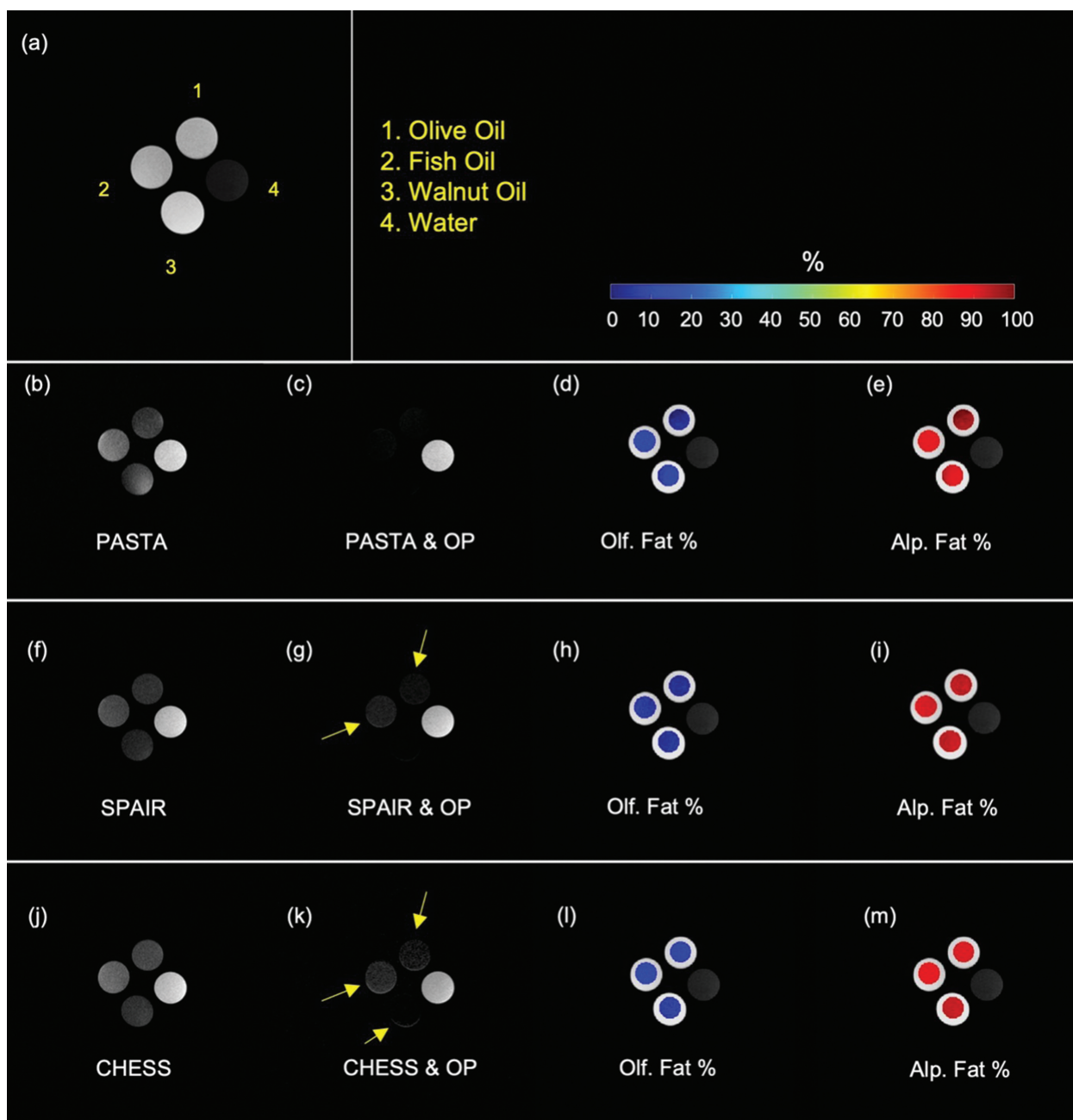
Fig. 4 In-phase image of (**a**) olive (1), fish (2), walnut (3) oils, and water (4) phantoms. Images acquired with (**b**) PASTA, (**c**) PASTA & OP, and the corresponding colormaps of (**d**) olefinic and (**e**) aliphatic fat fractions. (**f**) SPAIR, (**g**) SPAIR & OP with their fat fractions colormaps (**h** and **i**), (**j**) CHESS, (**k**) CHESS & OP with their fat fractions colormaps (**l** and **m**). Note the quality of fat suppression of PASTA & OP (**c**) compared to SPAIR & OP (**g**) and CHESS & OP (**k**), where remaining signal in oil phantoms is marked with yellow arrows. CHESS, chemical shift selective; OP, opposed phase; PASTA, polarity-altered spectral and spatial selective acquisition; SPAIR, spectral adiabatic inversion recovery.

aliphatic fat and water signals within a pixel, which, in orbits, may show not enough water cancellation with aliphatic fat signals. CHESS, SPAIR, and water excitation of PASTA show remaining fat signals. Note that SPAIR shows superior fat suppression as compared to CHESS- and PASTA-only acquisitions. However, among the images acquired with the combined fat suppression technique, PASTA & OP (**g**) demonstrates the best fat suppression in orbits with well-delineating optical nerve and extraocular muscles. All axial slices show well fat-suppressed images using the PASTA & OP technique.

Figure 4 demonstrates axial images of a phantom study. In-phase image (Fig. 4a) is with labels denoting olive (1), fish (2), walnut (3) oils, and a water phantom (4). Below, in

Table 2 Results of the olefinic fat fraction semi-quantification

Technique	Olive oil %	Fish oil %	Walnut oil %
NMR	06.0	12.6	11.5
PASTA	05.0 ± 1.6	12.8 ± 1.7	11.2 ± 2.1
SPAIR	05.7 ± 1.3	07.3 ± 1.6	06.4 ± 1.3
CHESS	10.8 ± 1.0	14.8 ± 1.8	08.6 ± 1.1

CHESS, chemical shift selective; NMR, nuclear magnetic resonance; PASTA, polarity-altered spectral and spatial selective acquisition; SPAIR, spectral adiabatic inversion recovery.
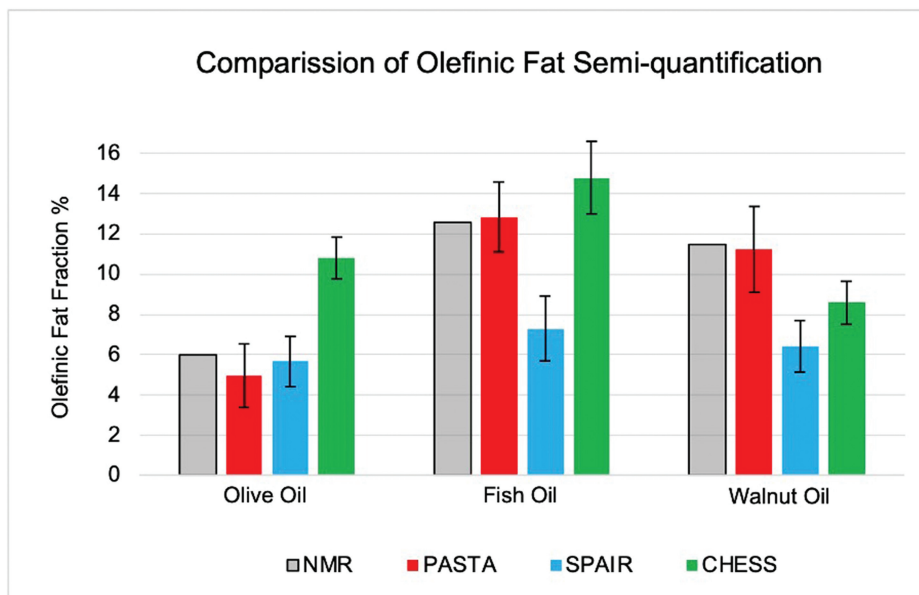

Fig. 5 Bar chart comparison of the olefinic fat fraction semi-quantification results with the results of 11.7T NMR measurements for olive, fish, and walnut oils. NMR results are plotted in gray, MRI results are given with pixel-wise standard deviation error bars, PASTA (and PASTA & OP) in red, SPAIR (and SPAIR & OP) in blue, and CHESS (CHESS & OP) in green. CHESS, chemical shift selective; NMR, nuclear magnetic resonance; OP, opposed phase; PASTA, polarity-altered spectral and spatial selective acquisition; SPAIR, spectral adiabatic inversion recovery.

each row, images are acquired using different fat suppression techniques with the derived olefinic and aliphatic fraction colormaps. Images and colormaps are from PASTA and PASTA & OP (Fig. 4b–e); fat signals in oils are somewhat suppressed in PASTA-only image (Fig. 4b) and an excellent level of fat suppression is achieved for all the oil phantoms with PASTA & OP (Fig. 4c). SPAIR and SPAIR & OP images with derived colormaps are presented in (Fig. 4f–i); note that among images acquired with a single fat sat technique only (Fig. 4b, f, and j), SPAIR demonstrates the best level of fat suppression. SPIAR & OP, although achieving a very good level of fat suppression, still has remaining signals in olive and fish oils and looks inferior to the PASTA & OP. The bottom row demonstrates images acquired with CHESS (Fig. 4j) and CHESS & OP (Fig. 4k) with the corresponding olefinic and aliphatic fat fraction colormaps (Fig. 4l and m). Note the remaining signal in each of the oil phantoms for CHESS & OP. Table 2 summarizes quantitative results for

olefinic and aliphatic fat fractions calculated for the ROIs, as shown in the colormaps of Fig. 4. To validate aliphatic and olefinic fat composition NMR spectrums for the extractions of the olive (Supplementary Fig. 1), fish (Supplementary Fig. 2), and walnut (Supplementary Fig. 3), oils were acquired at 11.7T. The spectrum at 11.7T NMR calculated below 3 ppm under the curves of each peak provides 6.5%, 12.6%, and 11.5% of olefinic fat of all fat signals under the curves for olive, fish, and walnut oils, respectively. All aliphatic fatty acid peaks below 3 ppm were summed together under the integrated curves, including methylene-interrupted double bond or diacyl, α-and β-carboxyl (-CO-CH_2-CH$_2$), α-olefinic next to a double bond (-CH_2-CH=CH-CH_2-), methylene (CH_2)$_n$, methyl (-CH$_3$) protons. The composition of unsaturated or olefinic (-CH=CH-) protons and aliphatic or saturated fatty acid was calculated. Figure 5 is a visual representation of the results listed in Table 2. Olefinic fat fractions calculated from PASTA and PASTA & OP images
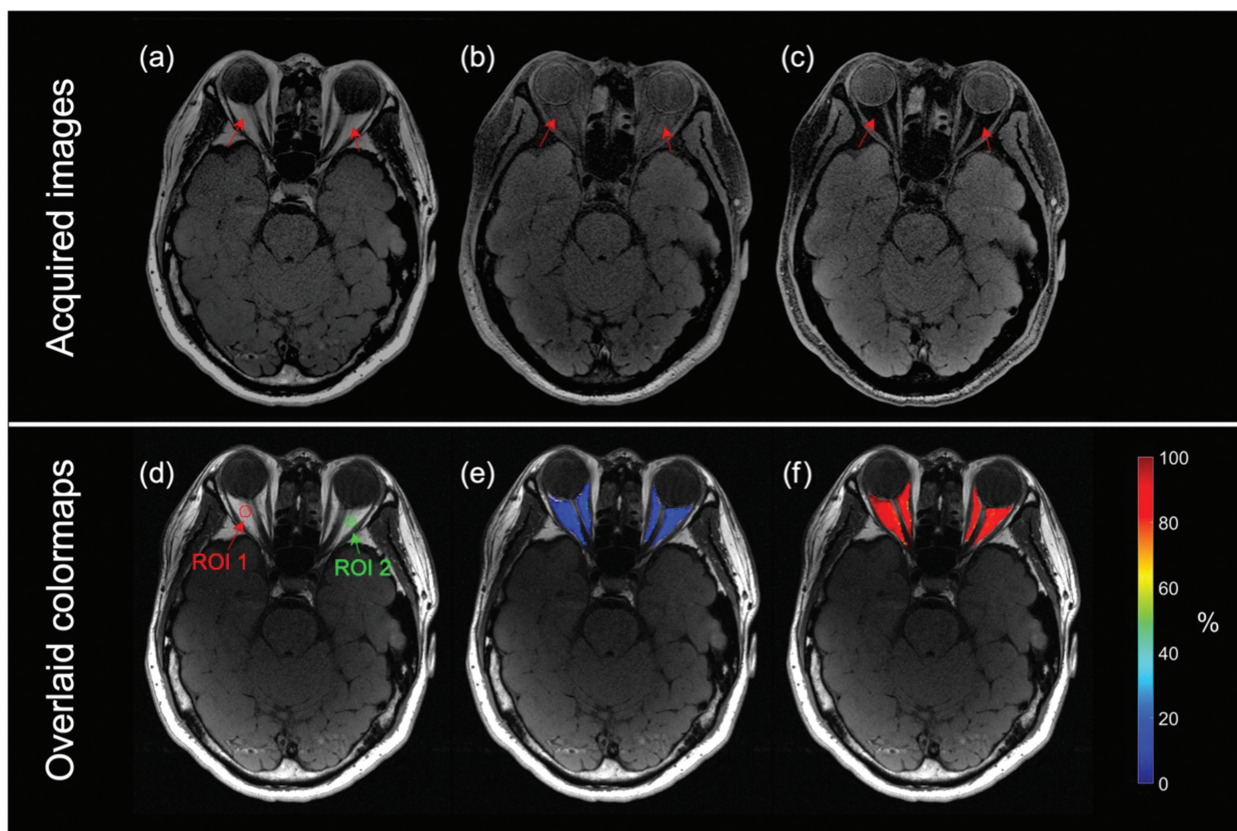
Fig. 6 Axial images for the same slice. Top panel: (**a**) in-phase (both water and fat) (here orbit fat is bright), (**b**) PASTA (water and unsaturated fat) (somewhat suppressed), and (**c**) PASTA with OP (only water) (complete suppression). Bottom panel: (**d**) in-phase image with superimposed ROIs used for fat fraction measurements, (**e** and **f**) colormaps of olefinic and aliphatic fat fractions, respectively, superimposed over in-phase image. The fat fractions were found to be (ROI 1) $F_{olf} = 12\%$, $F_{alp} = 88\%$; (ROI 2) $F_{olf} = 15\%$, and $F_{alp} = 85\%$. OP, opposed phase; PASTA, polarity-altered spectral and spatial selective acquisition.

Table 3 Average aliphatic/olefinic fat fractions and the ratio for 8 subjects

	F_{alp} %	F_{olf} %	F_{alp}/F_{olf}
ROI 1	90.3 ± 2.8	9.8 ± 2.8	10.1 ± 3.4
ROI 2	89.9 ± 4.8	10.1 ± 4.8	11.7 ± 6.6
Average	90.1 ± 3.8	9.9 ± 3.8	10.7 ± 5.1

(red bars) were in good agreement with the NMR measurements for each of the oil phantoms. Note a slight underestimation of the olefinic fat fraction in olive oil, however still within the range of standard diviation (SD) error. SPAIR and SPAIR & OP severely underestimated olefinic fat fraction for fish and walnut oil, yet demonstrated more accurate results for the olive oil. Fat fractions calculated from CHESS and CHESS & OP images were the least accurate.

For the human orbit study, a set of three images (In-phase, PASTA, and PASTA & OP) were acquired in all 8 subjects. Figure 6a–c shows these 3 sets of images: In-phase, PASTA, and PASTA & OP on one of the volunteers. The In-phase image shows both water and fat signals (Fig. 6a). PASTA-only with the water excitation gives incomplete fat suppression (Fig. 6b). PASTA & OP provides excellent fat-suppressed orbit image (Fig. 6c). Derived colormaps for fat fractions are shown in Fig. 6d–f. The olefinic fat in percentage, over both aliphatic and olefinic fat as 100%, was between 12% and 15%. ROI measurements averaged across all the participants are presented in Table 3. Olefinic fat was found to account for 9.9% of total fat while aliphatic fat fraction was 90.1%. The reproducibility study confirmed initial measurements resulting in standard deviations of 1.43 and 2.06 (for fat fraction % averaged across four measurements, two ROIs per acquisition). A slight mismatch can be attributed to the placement of the ROIs. This

result of aliphatic and olefinic composition in our measurements was similar to the excised tissue analysis of OAT from human orbits (Table 1). We have calculated the aliphatic and olefinic composition from their OAT to be 92.6%–94.5% aliphatic and 7.4%–5.5% olefinic fat composition, whereas our live OAT analysis using our technique provides about 90.1% aliphatic and 9.9% olefinic fatty acids.

Discussion

Several techniques have been previously applied for fat suppression in orbits with the primary goal to identify orbital lesions such as optic neuritis and to improve the visualization of the optical nerve.[16–19] Compared to the method presented here, each of the above studies used solely one of the following techniques per acquisition: Dixon,[16] CHESS, SPAIR, or STIR.[17–19] Although good and uniform fat suppression for orbit can be achieved with STIR, which, unlike Dixon and CHESS, is quite independent of magnetic field inhomogeneity, STIR comes at a cost of longer scan time or lower resolution. A combination of PASTA with opposed phase does not affect scan time yet still provides exceptional fat suppression in the orbit.

Regarding B_0 inhomogeneity of chemical selective fat suppression or water excitation like CHESS, SPAIR, and PASTA, we have used slice-selective shimming, called multislice off-resonance fat suppression (MSOFT).[20] The MSOFT shimming measures B_0 shifts of all slices in the z-direction in this case, and acquisitions are applied with these B_0 shifts accordingly. Therefore, we have experienced good fat-suppressed images in all slices of PASTA & OP.

Quantification of fatty acids has been previously done for bone marrow[7,8] and liver.[6,21] A simpler method introduced in the current study allows for non-invasive direct quantification of aliphatic (single-bonded) and olefinic (double-bonded) protons in the OAT. Experimental results on the phantom were confirmed by the results of a high-resolution NMR experiment and the measurements from the *in-vivo* study were in good agreement with prior analysis results of excised human orbit tissues.[11] The semi-quantification of orbit fat determined about 6%–18% of olefinic fat depending on 8 subjects. Orbit fat plays an important role in ocular physiology and oculomotricity. Several studies have previously reported age-related changes in the intra-orbital structures.[22,23] Direct measurement of semi-quantification of orbital fat may potentially provide an additional tool for the assessment of orbital pathology and age-related changes. Although our study consists of only 8 subjects with an age range between 22 and 75 (three elder subjects: 61, 72, and 75 y.o.), we noticed that older subjects (over 60 y.o.) showed less olefinic fat fraction than young subjects. We will continue investigating the age-related difference in olefinic fat composition that may be associated to geriatric eye diseases.

In terms of the technical advantages, we can directly measure the olefinic and aliphatic fat composition using three linked pulse sequences, whereas the CSE-MRI measures protons in different chemical shifts using a model spectrum from a small voxel in MRS, which is utilized for the estimation of the fat composition in the entire organ like liver and bone. As indicated in the recent review article, several limitations in quantification are reported such as MRS identification of each peak and estimation process of MRS to MRI.[14]

The study also has several limitations. (i) The reason for having residual saturated fat signal after the water excitation by PASTA is not well understood. A possible explanation could be a saturated fat signal evolved with uncoupled signals of a J-coupling effect in multiple refocusing pulses in FSE. These residual saturated fat signals could be canceled by near water olefinic fat (+0.5 ppm) and aliphatic fat (−3.5 ppm) opposed phase technique. The semi-quantification process does not account for a small aliphatic fat fraction remaining in PASTA-only image. We observed that SPAIR provides better fat suppression than PASTA (Fig. 3). (ii) There are possible errors in per voxel quantification at the edge of the orbits and near the optic nerve. Images were acquired with 2D FSE and only registered in plane, though image plane motion as well as arbitrary orbital muscle contraction were not taken into account. To minimize the impact of these factors, all the ROIs were placed in the large cross-sectional areas. (iii) PASTA utilizes a water excitation pulse with a relatively long duration that may result in susceptibility between tissue and air, e.g., around nasal cavity. However, image quality of PASTA & OP was not disturbed. (iv) The comparison between NMR and MRI results did not account for the scaling of individual components of the spectrum due to relaxation effects in MRI. T_1 relaxation times for the various fatty acids range from 154 ms to 543 ms while T_2 relaxation times range from 44 ms to 80 ms.[14] In the present study, all images were acquired with TE/TR = 15/1000 ms, making T_2 effect the major source of discrepancy when comparing the results of NMR and MRI semi-quantification. (v) Lastly, in our olefinic and aliphatic fat quantification, we did not count the backbone protons of triglycerides connecting three fatty acids, which are resonating near the water peak.

Conclusion

In this study, we have introduced an effective fat suppression technique that combines PASTA with opposed phase in the FSE sequence and have successfully applied it for the imaging of orbits. The method allows fast acquisition of human orbits with excellent fat suppression and simple semi-quantification of olefinic and aliphatic fat fractions. In the future, we would like to compare our method in patients with orbital diseases.

Further application of the developed technique can focus on studies with different anatomies and establishing biomarkers for certain conditions and regions, e.g., fatty liver disease, bone marrow, and brown fat in olefinic and aliphatic fatty composition.

Acknowledgments

Funding

Conflicts of Interest

The part of this result was presented at the ISMRM 2021. Mr. Yoshimori Kassai is an employee of Canon Medical Systems, Japan. The remaining coauthors have no conflicts of interest.

Supplementary Information

Supplementary files are available online.

Supplementary Fig. 1
11.7T NMR spectrum of the olive oil. Olefinic or unsaturated fat around 5.3 ppm is calculated to be about 6% of all fatty acids at 11.7T *in vitro* NMR.

Supplementary Fig. 2
11.7T NMR spectrum of the fish oil. Olefinic or unsaturated fat around 5.3 ppm is calculated to be about 12.6% of all fatty acids at 11.7T *in vitro* NMR.

Supplementary Fig. 3
11.7T NMR spectrum of the walnut oil. Olefinic or unsaturated fat around 5.3 ppm is calculated to be about 11.5% of all fatty acids at 11.7T *in vitro* NMR.

Appendix

Slice thickness L from bandwidth F_0 at central frequency and applied gradient G is given

$$\Delta S_0 = \frac{2\pi \cdot F_0}{\gamma \cdot G_0} \tag{A1}$$

Then, for water (w) and fat (f) when consecutive 90 and 180 pulses are applied

$$\Delta S_{w,f}^{90\&180} = \frac{2\pi}{\gamma} \left(\frac{F_{w,f}}{G_{90}} - \frac{F_{w,f}}{G_{180}} \right) \tag{A2}$$

The slice overlap ratio is given as

$$R = \frac{\Delta S - \delta S}{\Delta S} \tag{A3}$$

Where δS is slice separation

$$\delta S = \left| \Delta S_w^{90\&180} - \Delta S_f^{90\&180} \right| \tag{A4}$$

Using equation A2 to expand equation A4 and then plugging it into the equation A3

$$R = \left(\Delta S - \frac{2\pi}{\gamma} \left| \frac{\Delta F_{cs}}{G_{90}} - \frac{\Delta F_{cs}}{G_{180}} \right| \right) \cdot \frac{1}{\Delta S} \tag{A5}$$

Where ΔF_{cs} is chemical shift in Hz given as

$$\Delta F_{cs} = F_w - F_f \tag{A6}$$

Since the equation A1 can be re-written through the pulse duration τ

$$\Delta S_0 = \frac{2\pi}{\gamma \cdot G \cdot \tau_0} \tag{A7}$$

Recasting A7 for gradient G gives

$$G_0 = \frac{2\pi}{\gamma \cdot \Delta S_0 \cdot \tau_0} \tag{A8}$$

After plugging A8 to A5 and since the gradients corresponding to 90 and 180 RF pulses are of opposite polarity ($G_{90} = -G_{180}$), we arrive at final equation

$$R = 1 - |\Delta F_{cs}|(\tau_{90} + \tau_{180}) \tag{A9}$$

References

1. Zebardast N, Friedman DS, Vitale S. The prevalence and demographic associations of presenting near-vision impairment among adults living in the United States. Am J Ophthalmol 2017; 174:134–144.
2. Delfaut EM, Beltran J, Johnson G, Rousseau J, Marchandise X, Cotten A. Fat suppression in MR imaging: Techniques and pitfalls. Radiographics 1999; 19:373–382.
3. Yokoo T, Shiehmorteza M, Hamilton G, et al. Estimation of hepatic proton-density fat fraction by using MR imaging at 3.0T. Radiology 2011; 258:749–759.
4. Reeder SB, Hu HH, Sirlin CB. Proton density fat-fraction: A standardized MR-based biomarker of tissue fat concentration. J Magn Reson Imaging 2012; 36:1011–1014.
5. Tang A, Tan J, Sun M, et al. Nonalcoholic fatty liver disease: MR imaging of liver proton density fat fraction to assess hepatic steatosis. Radiology 2013; 267:422–431.
6. Leporq B, Lambert SA, Ronot M, Vilgrain V, Van Beers BE. Quantification of the triglyceride fatty acid composition with 3.0 T MRI. NMR Biomed 2014; 27:1211–1221.
7. Karampinos DC, Melkus G, Baum T, Bauer JS, Rummeny EJ, Krug R. Bone marrow fat quantification in the presence of trabecular bone: Initial comparison between water-fat imaging and single-voxel MRS. Magn Reson Med 2014; 71:1158–1165.
8. Karampinos DC, Ruschke S, Dieckmeyer M, et al. Quantitative MRI and spectroscopy of bone marrow. J Magn Reson Imaging 2018; 47:332–353.
9. Del Grande F, Santini F, Herzka DA, et al. Fat-suppression techniques for 3-T MR imaging of the musculoskeletal system. Radiographics 2014; 34:217–233.
10. Miyazaki M, Wheaton A, Kitane S. Enhanced fat suppression technique for breast imaging. J Magn Reson Imaging 2013; 38:981–986.

11. Sires BS, Lemke BN, Dortzbach RK, Gonnering RS. Characterization of human orbital fat and connective tissue. Ophthal Plast Reconstr Surg 1998; 14:403–414.

12. Miyazaki M, Takai H, Tokunaga Y, Hoshino T, Hanawa M. A polarity altered spectral and spatial selective acquisition technique. Proceedings of the 3rd Annual Meeting ISMRM, Nice, 1995; 657.

13. Fujimoto K, Okada T, Kido A, et al. Water fat opposed phase (WFOP) sequence is a robust fat suppression technique under the presence of B0 inhomogeneity in abdominal MRI at 3.0T. Proceedings of the 19th Annual Meeting ISMRM, Montreal, 2011; 2716.

14. Peterson P, Trinh L, Månsson S. Quantitative 1H MRI and MRS of fatty acid composition. Magn Reson Med 2021; 85:49–67.

15. Bydder M, Yokoo T, Hamilton G, et al. Relaxation effects in the quantification of fat using gradient echo imaging. Magn Reson Imaging 2008; 26:347–359.

16. Simon J, Szumowski J, Totterman S, et al. Fat-suppression MR imaging of the orbit. AJNR Am J Neuroradiol 1988; 9:961–968.

17. Borges AR, Lufkin RB, Huang AY, Farahani K, Arnold AC. Frequency-selective fat suppression MR imaging. J Neuroophthalmol 1997; 17:12–17.

18. Faizy TD, Broocks G, Frischmuth I, et al. Spectrally fat-suppressed coronal 2D TSE sequences may be more sensitive than 2D STIR for the detection of hyperintense optic nerve lesions. Eur Radiol 2019; 29:6266–6274.

19. Mukherji SK, Tart RP, Fitzsimmons J, et al. Fat-suppressed MR of the orbit and cavernous sinus: comparison of fast spin-echo and conventional spin-echo. AJNR Am J Neuroradiol 1994; 15:1707–1714.

20. Miyazaki M, Kojima F, Igarashi H. Uniform Fat Suppression in Multislice Imaging: A Multislice Off-Resonance Fat Suppression Technique (MSOFT). Proceedings of the 2nd Annual Meeting ISMRM, San Francisco,1994; 796.

21. Bydder M, Chavez T, Lam J, et al. Triglyceride saturation in patients at risk of NASH and NAFLD: A cross-sectional study. Biophysica 2021; 2:8–15.

22. Darcy SJ, Miller TA, Goldberg RA, Villablanca JP, Demer JL, Rudkin GH. Magnetic resonance imaging characterization of orbital changes with age and associated contributions to lower eyelid prominence. Plast Reconstr Surg 2008; 122:921–929.

23. Watanabe M, Buch K, Fujita A, Jara H, Qureshi MM, Sakai O. Quantitative MR imaging of intra-orbital structures: Tissue-specific measurements and age dependency compared to extra-orbital structures using multispectral quantitative MR imaging. Orbit 2017; 36:189–196.